HHS Public Access

Author manuscript

FASEB J. Author manuscript; available in PMC 2021 February 01.

Published in final edited form as:

FASEB J. 2020 February ; 34(2): 2011–2023. doi:10.1096/fj.201902063R.

SHIP-1, a Target of miR-155, Regulates Endothelial Cell Responses in Lung Fibrosis

Haiying Tang[1,2,#], **Jingwei Mao**[1,3,#], **Xujun Ye**[1], **Fengrui Zhang**[1], **William G. Kerr**[4], **Tao Zheng**[1], **Zhou Zhu**[1,*]

[1]Section of Allergy and Clinical Immunology, Yale University School of Medicine, 333 Cedar Street, TAC S469C, New Haven, CT 06510

[2]Department of Pulmonary and Critical Care Medicine, First Affiliated Hospital, Dalian Medical University, Dalian, China 116011

[3]Department of Gastroenterology, First Affiliated Hospital, Dalian Medical University, Dalian, China 116011

[4]Department of Microbiology and Immunology, SUNY Upstate Medical University, Syracuse, NY

Abstract

SHIP-1 is a target of miR-155, a pro-inflammatory factor. Deletion of the SHIP-1 gene in mice caused spontaneous lung inflammation and fibrosis. However, the role and function of endothelial miR-155 and SHIP-1 in lung fibrosis remain unknown. Using whole-body miR-155 knockout mice and endothelial cell-specific conditional miR-155 (VEC-Cre-miR-155, or VEC-miR-155) or SHIP-1 (VEC-SHIP-1) knockout mice, we assessed endothelial-mesenchymal transition (EndoMT) and fibrotic responses in bleomycin (BLM) induced lung fibrosis models. Primary mouse lung endothelial cells (MLEC) and human umbilical vein endothelial cells (HUVEC) with SHIP-1 knockdown were analyzed in TGF-β1 or BLM, respectively, induced fibrotic responses. Fibrosis and EndoMT were significantly reduced in miR-155KO mice and changes in EndoMT markers in MLEC after TGF-β1 stimulation confirmed the *in vivo* findings. Furthermore, lung fibrosis and EndoMT responses were reduced in VEC-miR-155 mice but significantly enhanced in VEC-SHIP-1 mice after BLM challenge. SHIP-1 knockdown in HUVEC cells resulted in enhanced EndoMT induced by BLM. Meanwhile, these changes involved the PI3K/AKT, JAK/STAT3 and SMAD/STAT signaling pathways. These studies demonstrate that endothelial miR-155 plays an important role in fibrotic responses in the lung through EndoMT. Endothelial SHIP-1 is essential in controlling fibrotic responses and SHIP-1 is a target of miR-155. Endothelial cells are an integral part in lung fibrosis.

[*]Corresponding author.

Author Contributions

Conception and design: ZZ, HYT; Acquisition, analysis, and interpretation of data for the work: HYT, JWM, XJY, FRZ, TZ, ZZ; Provided resources: WGK; Drafting the work or revising it critically for important intellectual content: HYT, JWM, ZZ, TZ, WGK.

[#]Contributed equally

Current Address: Dr. Zhou Zhu, zhou_zhu@brown.edu, Department of Molecular Microbiology and Immunology, Brown University Warren Alpert Medical School, 171 Meeting St. SFH 274, Providence, RI 02912

Author Disclosures

The authors have no financial conflicts.

Keywords

Phosphatase SHIP-1; miR-155; Endothelial-mesenchymal Transition; Lung Fibrosis

Introduction

Pulmonary fibrosis is characterized by aberrant accumulation of fibrotic tissue or scarring in the lung due to multiple causes. Idiopathic pulmonary fibrosis (IPF) is a chronic fibrosing interstitial lung disease with unknown etiology, poor prognosis and high mortality. Currently, treatment modalities for lung fibrosis, particularly IPF, are very limited.

Src Homology 2-containing Inositol Phosphatase-1 (SHIP-1) controls the intracellular levels of PI3K product PIP3 and functions as a negative regulator of cytokine and immune receptor signaling (1, 2). Deletion of the SHIP-1 gene in mice leads to an immunological phenotype with overproduction of pro-inflammatory cytokines, activation of myeloid cells, and severe inflammation in the lung (3, 4). Previous studies by our laboratory and others showed that whole-body SHIP-1 KO mice developed a type 2 like severe lung inflammation and lung fibrosis (5, 6). These studies demonstrated that SHIP-1 plays an important role in maintaining lung homeostasis.

MicroRNAs (miRNAs) play important roles in regulating gene expression and specific miRNAs participate in the fibrotic process in different tissues and organs (7–9). MiRNA-155 (miR-155), a pro-inflammatory factor via SHIP-1 down regulation, has been identified as having immune regulatory functions and plays a critical role in tissue fibrosis in liver and lung (10–13). However, contradictory effects of miR-155, pro-fibrotic and anti-fibrotic, in experimental and idiopathic pulmonary fibrosis have been reported (11, 14).

Several studies proposed the concept that lung endothelial cells and endothelial-mesenchymal transition (EndoMT) play important roles in the pathogenesis of pulmonary fibrosis (15–18). However, the role of endothelial cells and the function and relationship of endothelial miR-155 and SHIP-1 in lung fibrosis remain unknown. We hypothesized that endothelial miR-155 mediates fibrotic responses in the lung through EndoMT; Endothelial SHIP-1, a target of miR-155, is essential in controlling fibrotic responses in the lung.

Materials and Methods

Animals

Wild type (WT), miR-155 (Stock No. 007745) whole-body knockout (KO), Mir155 floxed (Stock No. 026700), and VEC-Cre (Stock No. 017968) mice on C57BL/6 genetic background were purchased from the Jackson Laboratory (Bar Harbor, ME). The SHIP-1 floxed mice on C57BL/6 background were generated as previously described (19). Endothelial cell specific conditional deletion of miR-155 or SHIP-1 in mice were generated by cross-breeding VEC-Cre mice with Mir155 floxed or SHIP-1 floxed mice to obtain VEC-Cre/miR-155 mice and VEC-Cre/SHIP-1 mice. Primers and PCR protocols for genotyping miR-155 KO and Mir155 floxed mice were the same as the original donating laboratories. The primers for VEC-Cre mice were: 5’-CCC AGG CTG ACC AAG CTG AG-3’ and 5’-

AGT GCG TTC GAA CGC TAG AGC CTG T-3'. All mice were housed under specific pathogen-free conditions and given ad libitum access to food and water. All procedures performed on mice were in accordance with the National Institutes of Health guidelines for humane treatment of animals and were approved by the Institutional Animal Care and Use Committee at Yale University.

Bleomycin Induced Pulmonary Fibrosis Model

Mice 6 – 10 weeks of age were used for all experiments. No difference between male and female mice was noticed. Age-matched WT mice, miR-155KO mice, VEC-Cre/miR-155 mice, VEC-Cre/SHIP-1 mice and littermate control mice were intratracheally administered with bleomycin (BLM) 3 mg/kg, i.t. (Teva Pharmaceuticals, North Wales, PA) dissolved in 50 μl of 0.9% saline or saline vehicle control at day 0. Mice were sacrificed and BAL and lung samples were collected 28 days after bleomycin challenge.

Hematoxylin and Eosin (H&E) Staining

Paraffin sections of lung tissues were stained with H&E for structural evaluation. Briefly, the sections were deparaffinized with xylene and rehydrated in gradient ethyl alcohol; and then slides were stained with hematoxylin for 2 min and washed with hot water (60°C) for 5 min and eosin staining for 1 min. Finally, the slides were dehydrated and mounted.

Masson's Trichrome Staining

The paraffin sections were stained with Masson's trichrome for fibrosis evaluation. Briefly, the sections were deparaffinized with xylene and rehydrated in gradient ethyl alcohol; and then slides were placed in Bouin Fluid at 56°C for 1h and washed with tap water for 5 min as well as Weigert's Iron Hematoxylin staining for 10 min. After staining in Trichrome for about 15 min, sections were placed in 1% acetic acid solution for 1 min. Finally, the slides were dehydrated and mounted. Five fields were randomly selected in each slide under microscopy (Olympus BX51).

Hydroxyproline Assay

Hydroxyproline assay was performed to estimate collagen deposition in tissues, as an index of fibrosis. Lung tissues (~200 mg) were homogenized in 6 N HCl, then incubated for 16 hrs at 110°C. After filtration with 3-mm filter paper, filtered homogenate, 50 μl each, was neutralized with 450 μl 2.2% NaOH in Citrate-Acetate Buffer. Chloramine-T-solution, Perchloric acid were added in sequence for 20 min individually at room temperature (RT), then Dimethyl benzaldehyde-solution was added for 20 min at 60°C. The absorbance of samples and standard were measured at 565 nm wavelength against blank on a microplate reader.

Isolation of Primary Murine Lung Endothelial Cells (MLEC)

Mice were sacrificed with overdose of anesthetic, lung tissues were excised and put in RPMI medium with 100 U/ml penicillin, 100 μg/ml streptomycin. After transferring lung to 100-mm dish containing1–2 ml of 0.1% collagenase (Roche, # 1088 785) in RPMI, lung tissues were cut to the smallest pieces possible with sharp scissors, and incubated in 30 ml 0.1%

collagenase/RPMI for 1 hr, with shaking at 37°C. After removing undigested tissue fragments with 130–150 μm tissue strainer (BELLCO, #1985–11300), and centrifuging at 1000 rpm for 5 min, the supernatant was discarded. The cell pellet was washed with growth media, re-suspended in growth medium, and then cultured at 37°C in T-75/T-175 flasks. Cells were cultured and small colonies of endothelial-like cells were observed. On day 5 or 6, first immune selection was performed. Briefly, after suspending the sheep anti-rat magnetic beads (DYNAL #100.07) in 100 μl of PBS with 2% FBS per 10 μl of beads, 10 μl (10 μg) of anti-mouse CD102 (ICAM-2) Ab (Pharmingen, #553325) was added and rocked at 4°C overnight. The beads were added to the cells and incubated at 4°C for 1 hr. By using magnetic holder (DYNAL,#MPC-S), the beads/cells were harvested and plated on 0.2% gelatin-coated flasks. After culture for 3–7 days, another immune-selection were performed using anti-mouse CD31 Ab (Pharmingen, #553369).

Primary Human Umbilical Vein Endothelial Cells (HUVECs)

HUVECs were provided by the Core Facility of the Yale University Vascular Biology & Therapeutics Program. HUVECs were isolated from de-identified human tissues under protocols approved by the Yale Human Investigations Committee, cultured in Medium 199 (M199) supplemented with 20% fetal bovine serum (FBS), 100 U/ml penicillin, 100 μg/ml streptomycin, and 2 mM L-glutamine supplemented with 50 mg/ml endothelial cell growth supplement (ECGS), and used between passages 1 – 5 for experiments.

SHIP-1 siRNA in HUVECs

SHIP-1 siRNA in HUVECs was performed according to Amaxa™ 4D-Nucleofector™ Protocol (Lonza Cologne GmbH, Cologne, Germany, Catalog #: V4XP-5012). Briefly, 2 days before Nucleofection, HUVECs were passaged and cultured at 37°C with 5% CO2. After trypsinization and centrifugation, cells were harvested and resuspended with 4DNucleofector™ Solution. Master mixes containing HUVECs, substrates (SHIP-1 siRNA or scrambled siRNA) and Nucleofector solution were prepared and transferred into the Nucleocuvette™ Vessels. Program CA-167 of the Nucleofection™ Process according to the protocol was performed. After completion of the run, HUVECs were suspended with pre-warmed medium, and incubated in humidified 37°C, 5% CO_2 incubator until analysis.

Immunofluorescence (IF)

Paraffin slides were used for IF staining of α-SMA, CD31 and VE-Cadherin. Samples were deparaffinized with xylene and rehydrated in gradient ethyl alcohol. Next, the samples were treated for antigen retrieval utilizing 0.1% trypsin for 20 min at 37°C. The sections were permeabilized with 0.3% Triton-X 100 and blocked with 5% donkey serum at RT. Following the blocking step, primary antibodies were applied, including mouse anti-α-SMA (1:300; Sigma-Aldrich, St. Louis, MO), rat anti-CD31 (1:100, BD Pharmingen, San Jose, CA) and goat anti-VE-cadherin (1:200; SCBT) and incubated overnight at 4°C. The sections were washed and incubated with secondary antibodies conjugated to Alexa Fluor 555 or 647 (1:300) for 30 min at RT. Samples were mounted with DAPI (Cell Signaling Technology, Danvers, MA) containing medium for nuclear staining.

IF staining of MLEC for α-SMA, CD31, VE-Cadherin and Vimentin. Cells were fixed with 0.5 ml of 4% paraformaldehyde and 0.5% triton-X-100 for 30 minutes at RT. Following the blocking step, primary antibodies, including mouse anti-α-SMA (1:300; Sigma), rat anti-CD31 (1:100, BD), goat anti-VE-cadherin (1:200; SCBT) and goat anti-Vimentin (1:20, Sigma) were applied and cells were incubated for 2 hrs at RT. Then cells were incubated with secondary antibodies conjugated to Alexa 555 or 647 (1:300) for 45 min at RT. Slides were mounted with DAPI medium and SlowFade Gold (Thermo Fisher Scientific, Waltham, MA).

Quantitative PCR (Q-PCR) of mRNA

Total RNA was extracted from lung tissues and MLECs using RNeasy Plus Mini Kit (QIAGEN, Germantown, MD). Sample mRNA was determined by Q-PCR using One-Step TB Green PrimeScript RT-PCR Kit II (Perfect Real Time) (Takara Bio USA Inc., Mountain View, CA, Cat#RR086A) according to the manufacturer's instructions. Q-PCR Primers for α-SMA, VE-Cadherin, Collagen I, Fibronectin, SHIP-1, GAPDH were shown in Table 1. Ct values of the indicated genes in each sample were calculated, and the transcript levels were calculated by the 2-ΔΔCt method. Endogenous Ct values of GAPDH were used as control.

Immunoblotting (IB or Western Blot) and Immunoprecipitation (IP)

Tissue and cell proteins were extracted using lysis buffer. Lysates were incubated on ice for 20 min, and the soluble fraction was isolated by centrifugation at 14,000 rpm for 10 min at 4°C. Protein concentration of the extracts was measured using the colorimetric Pierce BCA protein assay kit (Thermo Fisher Scientific, Waltham, MA). Equal amounts of proteins were loaded and separated by SDS-PAGE. Proteins transferred to 0.2-μm nitrocellulose membrane (Bio-Rad Laboratories) were analyzed by immunoblotting with primary antibodies, including mouse anti-α-SMA (1:5000, Sigma, St. Louis, MO), goat anti-VE-Cadherin (1:200, Santa Cruz Biotechnologies, Dallas, TX), rabbit anti-Collagen type I (1:5000, Abcam, Cambridge, MA), rabbit anti-Vimentin (1:1000, Cell Signaling Technology, Danvers, MA), mouse anti-CD31 (1:200) and mouse anti-HSP90 (1:1000, BD Biosciences, San Jose, CA), mouse anti-β-Actin (1: 2000, Santa Cruz Biotechnology, sc-47778). After washing with Tris buffered saline containing 0.1% Tween-20 (TBS/T), membranes were incubated with fluorophore-conjugated secondary antibodies (LI-COR, Lincoln, NE) having 680 nm or 800 nm emission. Proteins were visualized and quantified using the Odyssey Infrared Imaging System (LI-COR). HSP90 or β-Actin was used as a loading control.

Immunoprecipitation (IP) was performed using the Protein A/G PLUS-Agarose protocol (Santa Cruz Biotechnologies, Dallas, TX, sc-2003). Briefly, HUVECs were harvested in 2 ml RIPA buffer, cleaved on ice for 30 min, centrifuged at 12,000g for 30 min, and the supernatant was stored for further analysis. SHIP-1 antibody (Santa Cruz Biotechnologies, sc-8425) and protein A/G beads were added to the cell lysis and incubated overnight at 4°C with shaking. After centrifugation at 3,000g for 5 min at 4°C, the supernatant was carefully aspirated. Protein A/G–beads were washed 3–4 times with RIPA buffer and collected. Then, SDS loading buffer was added and the samples were boiled for 10 minutes for immunoblotting analysis as described above.

Statistical analysis

Data were analyzed with GraphPad Prism 5 (GraphPad Software, San Diego, CA). Student's *t* test was used to compare between groups. One-way ANOVA was used to test the differences among three or more groups. Differences with $p < 0.05$ were considered statistically significant. Data were expressed as Mean±SD unless otherwise indicated.

Results

Endothelia-Mesenchymal Transition (EndoMT) in BLM-induced lung fibrosis

To determine whether EndoMT was involved in the process of lung fibrosis, we analyzed changes of endothelial and fibrotic markers in the lung of WT mice 28 days after BLM challenge (WT-BLM). In lung histology, H&E and Trichrome staining showed that all normal saline control mice (WT-NS) had no abnormalities while significant collagen deposition was seen in the lung tissues of WT-BLM mice (Figure 1A). Q-PCR analysis showed increased α-SMA mRNA but decreased VE-cadherin mRNA in the lung of WT-BLM mice compared to WT-NS controls (Figure 1B). Using specific antibodies, immunofluorescence demonstrated significantly increased α-SMA but decreased VE-cadherin and CD31 in the lung sections of WT-BLM mice (Figure 1D, E). These results indicate that EndoMT occurred in BLM induced lung fibrosis.

MiR-155 gene deletion alleviated lung fibrotic response and EndoMT

MiR-155 has been identified as having immune regulatory functions and plays a critical role in tissue fibrosis. However, opposing effects of miR-155, anti-fibrotic and fibrotic, have been reported in lung fibrosis. To clarify the role of miR-155, we utilized miR-155 whole-body knockout mice and endothelial specific conditional knockout mice to assess the fibrotic and endothelial responses in BLM induced lung fibrosis models. In the lung of miR-155KO-BLM mice, tissue fibrosis, hydroxyproline content, collagen I and α-SMA were assayed by histology, Q-PCR, and immunoblot. H&E and Trichrome staining showed less fibrosis and collagen deposition in the lung of miR-155 KO-BLM mice compared to WT mice (Figure 2A). Measurements of hydroxyproline content and Q-PCR of Collagen I mRNA showed both were significantly decreased in miR-155KO-BLM lung tissues (Figure 2B, C). As shown in Figure 2D, significantly decreased levels of α-SMA and Collagen I proteins by Western blot were found in the lung tissues of miR-155KO-BLM mice. Furthermore, EndoMT responses in miR-155KO mice were significantly inhibited, with lower levels of α-SMA but higher CD31 and VE-cadherin, compared to WT-BLM mice (Figure 2E-G).

Endothelial miR-155 mediates lung fibrosis through regulating EndoMT

To delineate the specific cell types that contribute to the observed changes in EndoMT in miR-155KO mice, we assessed fibrotic and EndoMT markers in isolated mouse lung endothelial cells (MLEC) from WT and miR-155KO mice. We found that Fibronectin mRNA was significantly decreased but VE-cadherin mRNA was increased in the primary MLEC from miR-155KO mice after TGF-β1 stimulation for 24 hrs compared to WT-MLEC (Figure 3A, B). As shown in Figure 3C-E, changes in EndoMT markers α-SMA, Vimentin, VE-cadherin and CD31 in isolated primary MLEC from WT and miR-155KO mice after

TGF-β1 stimulation for 72 hrs confirmed the findings that miR-155 gene deletion reduced EndoMT *in vivo*.

To further confirm the role of endothelial miR-155 in lung fibrosis, we generated mice with endothelial cell-specific conditional deletion of miR-155 (VEC-Cre/miR-155 or VEC-miR-155 mice) and assessed their endothelial responses in BLM induced lung fibrosis models. As shown in Figure 3F, endothelial specific conditional deletion of miR-155 led to less fibrosis and collagen deposition in BLM induced lung fibrosis model. The levels of collagen I mRNA and protein also decreased in VEC-miR-155-BLM lung tissues (Figure 3G, H). Comparing with WT-BLM mice, endothelial marker, VE-cadherin was increased whereas mesenchymal marker, α-SMA, decreased in VEC-miR-155-BLM lung tissue (Figure 3H, I). Taken together, these data clearly demonstrate that endothelial cell-specific deletion of miR-155 resulted in similar responses as seen in miR-155KO mice after BLM challenge, indicating that endothelial miR-155 mediated lung fibrosis.

Lack of endothelial SHIP-1 facilitated lung fibrosis and EndoMT in vivo

Our previous work showed that mice lacking SHIP-1 had severe lung inflammation and fibrosis (5). We thought that SHIP-1, as a target of miR-155, might participate in regulating fibrotic and EndoMT responses in BLM-induced lung fibrosis. We determined the protein levels of SHIP-1 in lung tissues using Western blot. At steady state, SHIP-1 levels in miR-155KO and VEC-miR-155 mice were higher, compared to WT mice. After BLM challenge for 28 days, SHIP-1 levels decreased in all groups, but remained higher in miR-155KO and VEC-miR-155 mouse lungs than in WT mouse lungs (Figure 4A). Then, we confirmed that endothelial cells (HUVEC) expressed SHIP-1 and the levels of SHIP-1 were higher in primary MLEC from miR-155KO mice comparing with those in WT mice without TGF-β1 stimulation (Figure 4C, D). We generated mice with endothelial cell-specific conditional deletion of SHIP-1 (VEC-SHIP-1) and tested the response of these mice in the BLM model of lung fibrosis. H&E and Trichrome staining showed endothelial deletion of SHIP-1 led to more fibrosis and collagen deposition in BLM induced mice comparing to WT mice (Figure 4E). The levels of collagen I and α-SMA significantly increased but the level of VE-cadherin decreased in VEC-SHIP-1-BLM mice compared to WT-BLM mice (Figure 4F, G). As shown in Figure 4H and 4I, in VEC-SHIP-1 mice, α-SMA was increased, while VE-cadherin decreased, compared to WT mice.

SHIP-1 regulated TGF-β1 induced EndoMT in endothelial cells

Mouse lung endothelial cells (MLECs) from WT and VEC-SHIP-1 mice were isolated to clarify the role of SHIP-1 in the process of EndoMT. Cells were sorted with immunomagnetic beads and identified as endothelial cells by FACS and Western blot (Figure 5A, B). After TGF-β1 stimulation for 72 hrs, EndoMT markers in lung endothelial cells were analyzed. IF staining showed endothelial markers, VE-cadherin and CD31 decreased, while mesenchymal markers, α-SMA and Vimentin increased in VEC-SHIP-1 MLECs compared to WT MLECs (Figure 5C, D). Western-blot results also demonstrated similar changes in VE-cadherin, α-SMA and Vimentin in WT and VEC-SHIP-1 MLECs as shown in Figure 5E. Taken together, changes in EndoMT markers in primary MLECs from WT and VEC-SHIP-1 mice after TGF-β1 stimulation confirmed the *in vivo* findings.

Furthermore, knockdown of SHIP-1 in primary HUVECs showed CD31 expression decreased but α-SMA increased when stimulated with BLM (Figure 5F), indicating enhanced EndoMT.

Endothelial miR-155 and SHIP-1 in pulmonary fibrosis involving the PI3K/AKT, STAT3 and SMAD/STAT signaling pathways

To determine which signaling pathways were involved in endothelial miR-155 and SHIP-1 regulation of pulmonary fibrotic responses, we analyzed the expression and activation of signaling molecules PI3K/AKT as well as STAT3 and SMAD/STAT in the lung tissues of WT, miR-155KO, VEC-miR-155 and VEC-SHIP-1 mice 28 days after BLM challenge. Western blot results showed that, compared to WT mice, miR-155KO and VEC-miR-155 mice had significantly reduced activation or expression of p-Akt, Twist, Snail, p-STAT3, p-Smad2 and p-Smad3 in the lung (Figure 6A-D). In contrast, VEC-SHIP-1 mice showed significantly enhanced activation or expression of fibrotic signaling molecules p-Akt, Twist, Snail, p-STAT3, p-Smad2 and p-Smad3, compared to those in WT mice (Figure 6E-F).

Discussion

IPF is a progressive, chronic and ultimately fatal interstitial lung disease characterized by enhanced extracellular matrix deposition. Although the exact etiology in IPF is unclear, complex, and probably diverse, previous studies have identified EndoMT as one of the important processes for the establishment and progression of the fibrotic changes (20–22). In our study, we also found that all control groups showed no abnormalities, while WT-BLM mice showed significant fibrotic responses in the lung; these were accompanied by decreased endothelial markers VE-cadherin and CD31 but increased mesenchymal cell marker α-smooth muscle actin (α-SMA), indicating EndoMT. Recent studies have demonstrated that myofibroblasts are the cells ultimately responsible for the severe organ fibrotic process such as in pulmonary fibrosis (23–25). Activated myofibroblasts can originate from various cell sources including endothelial cells that have acquired a mesenchymal phenotype through EndoMT (26, 27).

Emerging evidence has shown that diverse mediators such as TGF-β1, TNF-α, IL-1β, β-catenin, Akt/NF-κB, snail and so on, tightly control the process of EndoMT in fibrotic diseases (28). Among these factors, microRNA (miRNAs) are critical regulators, with the capacity to target multiple messenger RNAs involved in the EndoMT process and disease progression regulation (29). MiR-155 is a key mediator in the process of pulmonary fibrosis, besides in other lung diseases as allergic airway inflammation (30), lung injury (31), and lung cancer (32). However, opposing effects of miR-155, anti-fibrotic or fibrotic, in experimental and idiopathic pulmonary fibrosis have been reported (11, 14). The seemingly contradictory findings on miR-155 in these studies may have been the results of different study design and use of different cells, cytokines and pathways and at different stage of the disease. To further clarify the role of miR-155, we utilized miR-155 whole-body KO mice and assessed their endothelial responses in BLM induced lung fibrosis models. Our result demonstrated that miR-155 gene deletion alleviated lung fibrotic and EndoMT responses *in vivo*. Furthermore, isolated primary MLEC from WT and miR-155 KO mice after TGF-β1

stimulation confirmed *in vivo* findings that miR-155 gene deletion inhibited EndoMT. To determine the miR-155 contribution to the EndoMT response, we generated mice with endothelial cell-specific conditional deletion of miR-155 and assessed their responses in BLM induced lung fibrosis. The data clearly showed endothelial cell-specific deletion of miR-155 resulted in similar responses in miR-155KO mice after BLM challenge, indicating that endothelial miR-155 mediated lung fibrosis.

SHIP-1 is a negative regulator of cell signaling in a variety of hematopoietic cells through phosphoinositide; and it dephosphorylates PIP3 to PI-3,4-bisphosphate, effectively reducing or terminating the downstream signaling of the PI3K pathway (33). SHIP-1 participates in the process of several lung diseases such as asthma, lung injury and COPD (5, 34, 35). Evidence showed that SHIP-1 KO mice develop a series of pathologies characterized by progressive non-resolving lung inflammation, fibrosis, and emphysema (34). Our previous work also showed mice lacking SHIP-1 had severe lung inflammation and fibrosis (5). Of interest, SHIP-1 has been recognized as a target of miR-155 (36). However, the expression and the functional role of SHIP-1 in endothelial cells are unknown. To further study SHIP-1in regulating lung fibrotic response, we first determined the SHIP-1 expression in endothelial cells. Indeed, human umbilical vein endothelial cells (HUVEC) as well as mouse lung endothelial cells (MLEC) expressed SHIP-1. Our results also showed that SHIP-1 expression was upregulated in primary MLEC from miR-155KO mice, and importantly, lack of SHIP-1 in endothelial cells facilitated lung fibrosis.

Since miR-155 was involved in EndoMT in lung fibrosis, we reasoned that SHIP-1, as a target of miR-155, also participated in regulating EndoMT response. As shown in Figure 4F-I, in VEC-SHIP-1 mice, mesenchymal marker α-SMA was significantly increased, while endothelial marker VE-cadherin decreased, indicating that endothelial SHIP-1 is required in regulating EndoMT *in vivo*. Changes in EndoMT markers in isolated primary MLECs from WT and VEC-SHIP-1 mice stimulated with TGF-β1 confirmed the *in vivo* findings. Furthermore, knockdown of SHIP-1 in HUVEC resulted in decreased CD31 expression but increased α-SMA when stimulated with BLM (Figure 5F), showing enhanced EndoMT. Taken together, endothelial miR-155 regulates lung fibrotic and EndoMT responses by targeting SHIP-1 as one likely mechanism.

MiR-155 and SHIP-1 have essential roles in controlling hematopoietic cell functions through modulating PI3K signaling pathways essential for cell survival, proliferation, invasion and migration (37, 38). Studies found that inhibition of miR-155 potentially suppresses JAK/STAT and PI-3K-mediated cytokine signaling by its direct target SHIP-1 in post-stroke inflammatory responses (39). However, no report has identified the signaling pathways regarding endothelial miR-155 and SHIP-1 in regulating EndoMT during pulmonary fibrotic responses.

In assessing signaling pathways involved, we detected activation of signaling molecules PI3K/Akt, JAK/STAT3, Smad2/3 in WT, miR-155KO, VEC-miR-155 and VEC-SHIP-1 mouse lungs after BLM challenge. Our results showed that miR-155KO and VEC-miR-155 mice had significantly reduced activation or expression of p-Akt, Twist, Snail, p-STAT3, p-Smad2 and p-Smad3 (Figure 6A-D), whereas VEC-SHIP-1 mice showed the opposite,

significantly enhanced activation of fibrotic signaling molecules p-Akt, Twist, Snail, p-STAT3, p-Smad2 and p-Smad3 (Figure 6E, F). Our study revealed that through activation of PI3K/Akt signaling, the level of Twist increased correspondingly. Evidence indicates that the PI3K/Akt pathway predominantly regulates Twist phosphorylation (40); and the PI3K/AKT/Twist signaling pathway was involved in EndoMT induction. Snail, one of the EndoMT mediators, is essential for EndoMT and regulates the formation of endocardial cushion (41); and Snail acts as a transcriptional repressor of VE-cadherin when it is induced in endothelial cells during EndoMT (42). We found in this study that the expression of Snail was upregulated and p-Akt was simultaneously increased in VEC-SHIP-1 fibrotic lung tissues, suggesting that SHIP-1 participates in regulation of the Akt/Snail signaling pathway in lung fibrotic responses. Based on these findings, it is likely that hyper-activation of PI3K/Akt, a result of reduced dephosphorylation of PI (3, 4, 5)-P3 due to endothelial SHIP-1 deletion, is responsible for the induction of EndoMT in lung fibrotic responses.

The role of Smad2 and Smad3 in TGF-β1-induced EndoMT was documented in different types of endothelial cells (43); meanwhile, inhibition of EndoMT by SIS3, a Smad3 inhibitor, has been reported to attenuate the development of fibrosis in diabetic nephropathy (44). Our study showed that miR-155 and SHIP-1 are involved in activation and regulation, respectively, of TGF-β1 induced Smad2/3 and EndoMT responses in endothelial cells and in lung fibrosis. The underlying regulatory mechanisms need to be further investigated.

The JAK/STAT signaling pathway is essential in mediating cytokine signaling and there is cross-talk among the JAK/STAT signaling pathway and the PI3 kinase pathway and the TGF-β1 signaling pathway (45). The role of STAT3 in pulmonary fibrosis is not well defined, though activation of STAT3 has been associated with IPF disease progression (46). It was reported in mouse cortical tissues in a post-stroke inflammation model that the level of miR-155 positively, whereas that of SHIP-1 inversely, correlated with the status of STAT3 phosphorylation (39). We observed in this study that changes in miR-155 and SHIP-1 corresponded to the activation status of STAT3 in a similar pattern, indicating an interaction among miR-155, SHIP-1 and STAT3, perhaps through the PI3 kinase pathway.

In this study, we demonstrate that endothelial miR-155 plays an important role in mediating fibrotic responses in the lung through EndoMT; endothelial SHIP-1, a target of miR-155, is essential in controlling fibrotic responses through regulating the PI3K/Akt and JAK/STAT signaling pathways; and endothelial cells are an integral part in lung fibrosis.

Acknowledgement

This work was partially supported by NIH grant P01-HL107151 to ZZ and National Natural Science Foundation of China (NSFC) grant 81700066 to HYT.

Nonstandard abbreviations

α-SMA	Alpha-smooth muscle actin
BAL	Bronchoalveolar Lavage
BLM	Bleomycin

COPD	Chronic Obstructive Pulmonary Disease
Cre	Cre Recombinase
DAPI	4′,6-diamidino-2-phenylindole
ECGS	Endothelial Cell Growth Supplement
EndoMT	Endotheial-Mesenchymal Transition
FACS	Fluorescence-Activated Cell Sorting or Flow Cytometry
H&E	Hematoxylin and eosin
HUVEC	Human Umbilical Vein Endothelial Cells
IB	Immunoblot
IF	Immunfluorescence
IPF	Idiopathic Pulmoanry Fibrosis
KO	Knockout
miR	MicroRNA
MLEC	Mouse Lung Endothelial Cells
NS	Nornal Saline
SHIP-1	Src homology 2 (SH2) domain containing inositol polyphosphate 5-phosphatase 1
VEC	Vascular Endothelial Cadherin or VE-Cadherin
WT	Wildtype

References

1. Eramo MJ, and Mitchell CA (2016) Regulation of PtdIns(3,4,5)P3/Akt signalling by inositol polyphosphate 5-phosphatases. Biochem Soc Trans 44, 240–252 [PubMed: 26862211]
2. Fernandes S, Srivastava N, Sudan R, Middleton FA, Shergill AK, Ryan JC, and Kerr WG (2018) SHIP1 Deficiency in Inflammatory Bowel Disease Is Associated With Severe Crohn's Disease and Peripheral T Cell Reduction. Front Immunol 9, 1100 [PubMed: 29872435]
3. Helgason CD, Damen JE, Rosten P, Grewal R, Sorensen P, Chappel SM, Borowski A, Jirik F, Krystal G, and Humphries RK (1998) Targeted disruption of SHIP leads to hemopoietic perturbations, lung pathology, and a shortened life span. Genes Dev 12, 1610–1620 [PubMed: 9620849]
4. Liu Q, Oliveira-Dos-Santos AJ, Mariathasan S, Bouchard D, Jones J, Sarao R, Kozieradzki I, Ohashi PS, Penninger JM, and Dumont DJ (1998) The inositol polyphosphate 5-phosphatase ship is a crucial negative regulator of B cell antigen receptor signaling. J Exp Med 188, 1333–1342 [PubMed: 9763612]
5. Oh SY, Zheng T, Bailey ML, Barber DL, Schroeder JT, Kim YK, and Zhu Z (2007) Src homology 2 domain-containing inositol 5-phosphatase 1 deficiency leads to a spontaneous allergic inflammation in the murine lung. J Allergy Clin Immunol 119, 123–131 [PubMed: 17208593]

6. Duan M, Li WC, Vlahos R, Maxwell MJ, Anderson GP, and Hibbs ML (2012) Distinct macrophage subpopulations characterize acute infection and chronic inflammatory lung disease. J Immunol 189, 946–955 [PubMed: 22689883]
7. Li H, Zhao X, Shan H, and Liang H (2016) MicroRNAs in idiopathic pulmonary fibrosis: involvement in pathogenesis and potential use in diagnosis and therapeutics. Acta Pharm Sin B 6, 531–539 [PubMed: 27818919]
8. Stolzenburg LR, and Harris A (2018) The role of microRNAs in chronic respiratory disease: recent insights. Biol Chem 399, 219–234 [PubMed: 29148977]
9. Bagnato G, Roberts WN, Roman J, and Gangemi S (2017) A systematic review of overlapping microRNA patterns in systemic sclerosis and idiopathic pulmonary fibrosis. Eur Respir Rev 26
10. Artlett CM, Sassi-Gaha S, Hope JL, Feghali-Bostwick CA, and Katsikis PD (2017) Mir-155 is overexpressed in systemic sclerosis fibroblasts and is required for NLRP3 inflammasome-mediated collagen synthesis during fibrosis. Arthritis Res Ther 19, 144 [PubMed: 28623945]
11. Kurowska-Stolarska M, Hasoo MK, Welsh DJ, Stewart L, McIntyre D, Morton BE, Johnstone S, Miller AM, Asquith DL, Millar NL, Millar AB, Feghali-Bostwick CA, Hirani N, Crick PJ, Wang Y, Griffiths WJ, McInnes IB, and McSharry C (2017) The role of microRNA-155/liver X receptor pathway in experimental and idiopathic pulmonary fibrosis. J Allergy Clin Immunol 139, 1946–1956 [PubMed: 27746237]
12. Blaya D, Aguilar-Bravo B, Hao F, Casacuberta-Serra S, Coll M, Perea L, Vallverdu J, Graupera I, Pose E, Llovet L, Barquinero J, Cubero FJ, Caballeria J, Gines P, and Sancho-Bru P (2018) Expression of microRNA-155 in inflammatory cells modulates liver injury. Hepatology
13. Csak T, Bala S, Lippai D, Kodys K, Catalano D, Iracheta-Vellve A, and Szabo G (2015) MicroRNA-155 Deficiency Attenuates Liver Steatosis and Fibrosis without Reducing Inflammation in a Mouse Model of Steatohepatitis. PLoS One 10, e0129251
14. Christmann RB, Wooten A, Sampaio-Barros P, Borges CL, Carvalho CR, Kairalla RA, Feghali-Bostwick C, Ziemek J, Mei Y, Goummih S, Tan J, Alvarez D, Kass DJ, Rojas M, de Mattos TL, Parra E, Stifano G, Capelozzi VL, Simms RW, and Lafyatis R (2016) miR-155 in the progression of lung fibrosis in systemic sclerosis. Arthritis Res Ther 18, 155 [PubMed: 27377409]
15. Hartopo AB, Arfian N, Nakayama K, Suzuki Y, Yagi K, and Emoto N (2018) Endothelial-derived endothelin-1 promotes pulmonary vascular remodeling in bleomycin-induced pulmonary fibrosis. Physiol Res 67, S185–S197 [PubMed: 29947539]
16. Jimenez SA, and Piera-Velazquez S (2016) Endothelial to mesenchymal transition (EndoMT) in the pathogenesis of Systemic Sclerosis-associated pulmonary fibrosis and pulmonary arterial hypertension. Myth or reality? Matrix Biol 51, 26–36 [PubMed: 26807760]
17. Bacha NC, Blandinieres A, Rossi E, Gendron N, Nevo N, Lecourt S, Guerin CL, Renard JM, Gaussem P, Angles-Cano E, Boulanger CM, Israel-Biet D, and Smadja DM (2018) Endothelial Microparticles are Associated to Pathogenesis of Idiopathic Pulmonary Fibrosis. Stem Cell Rev 14, 223–235
18. Cao Z, Ye T, Sun Y, Ji G, Shido K, Chen Y, Luo L, Na F, Li X, Huang Z, Ko JL, Mittal V, Qiao L, Chen C, Martinez FJ, Rafii S, and Ding BS (2017) Targeting the vascular and perivascular niches as a regenerative therapy for lung and liver fibrosis. Sci Transl Med 9
19. Wang JW, Howson JM, Ghansah T, Desponts C, Ninos JM, May SL, Nguyen KH, Toyama-Sorimachi N, and Kerr WG (2002) Influence of SHIP on the NK repertoire and allogeneic bone marrow transplantation. Science 295, 2094–2097 [PubMed: 11896280]
20. Piera-Velazquez S, Mendoza FA, and Jimenez SA (2016) Endothelial to Mesenchymal Transition (EndoMT) in the Pathogenesis of Human Fibrotic Diseases. J Clin Med 5
21. Ursoli Ferreira F, Eduardo Botelho Souza L, Hassibe Thome C, Tomazini Pinto M, Origassa C, Salustiano S, Marcel Faca V, Olsen Camara N, Kashima S, and Tadeu Covas D (2019) Endothelial Cells Tissue-Specific Origins Affects Their Responsiveness to TGF-beta2 during Endothelial-to-Mesenchymal Transition. Int J Mol Sci 20
22. Lv Z, Wang Y, Liu YJ, Mao YF, Dong WW, Ding ZN, Meng GX, Jiang L, and Zhu XY (2018) NLRP3 Inflammasome Activation Contributes to Mechanical Stretch-Induced Endothelial-Mesenchymal Transition and Pulmonary Fibrosis. Crit Care Med 46, e49–e58 [PubMed: 29088003]

23. Lehtonen ST, Veijola A, Karvonen H, Lappi-Blanco E, Sormunen R, Korpela S, Zagai U, Skold MC, and Kaarteenaho R (2016) Pirfenidone and nintedanib modulate properties of fibroblasts and myofibroblasts in idiopathic pulmonary fibrosis. Respir Res 17, 14 [PubMed: 26846335]
24. Goodwin J, Choi H, Hsieh MH, Neugent ML, Ahn JM, Hayenga HN, Singh PK, Shackelford DB, Lee IK, Shulaev V, Dhar S, Takeda N, and Kim JW (2018) Targeting Hypoxia-Inducible Factor-1alpha/Pyruvate Dehydrogenase Kinase 1 Axis by Dichloroacetate Suppresses Bleomycin-induced Pulmonary Fibrosis. Am J Respir Cell Mol Biol 58, 216–231 [PubMed: 28915065]
25. Yazdani S, Bansal R, and Prakash J (2017) Drug targeting to myofibroblasts: Implications for fibrosis and cancer. Adv Drug Deliv Rev 121, 101–116 [PubMed: 28720422]
26. Abu El-Asrar AM, De Hertogh G, van den Eynde K, Alam K, Van Raemdonck K, Opdenakker G, Van Damme J, Geboes K, and Struyf S (2015) Myofibroblasts in proliferative diabetic retinopathy can originate from infiltrating fibrocytes and through endothelial-to-mesenchymal transition (EndoMT). Exp Eye Res 132, 179–189 [PubMed: 25637870]
27. Yin Q, Wang W, Cui G, Yan L, and Zhang S (2018) Potential role of the Jagged1/Notch1 signaling pathway in the endothelial-myofibroblast transition during BLM-induced pulmonary fibrosis. J Cell Physiol 233, 2451–2463 [PubMed: 28776666]
28. Cho JG, Lee A, Chang W, Lee MS, and Kim J (2018) Endothelial to Mesenchymal Transition Represents a Key Link in the Interaction between Inflammation and Endothelial Dysfunction. Front Immunol 9, 294 [PubMed: 29515588]
29. Kim J (2018) MicroRNAs as critical regulators of the endothelial to mesenchymal transition in vascular biology. BMB Rep 51, 65–72 [PubMed: 29353599]
30. Johansson K, Malmhall C, Ramos-Ramirez P, and Radinger M (2017) MicroRNA-155 is a critical regulator of type 2 innate lymphoid cells and IL-33 signaling in experimental models of allergic airway inflammation. J Allergy Clin Immunol 139, 1007–1016 e1009 [PubMed: 27492144]
31. Wang W, Liu Z, Su J, Chen WS, Wang XW, Bai SX, Zhang JZ, and Yu SQ (2016) Macrophage micro-RNA-155 promotes lipopolysaccharide-induced acute lung injury in mice and rats. Am J Physiol Lung Cell Mol Physiol 311, L494–506 [PubMed: 27371731]
32. Van Roosbroeck K, Fanini F, Setoyama T, Ivan C, Rodriguez-Aguayo C, Fuentes-Mattei E, Xiao L, Vannini I, Redis RS, D'Abundo L, Zhang X, Nicoloso MS, Rossi S, Gonzalez-Villasana V, Rupaimoole R, Ferracin M, Morabito F, Neri A, Ruvolo PP, Ruvolo VR, Pecot CV, Amadori D, Abruzzo L, Calin S, Wang X, You MJ, Ferrajoli A, Orlowski R, Plunkett W, Lichtenberg TM, Davuluri RV, Berindan-Neagoe I, Negrini M, Wistuba II, Kantarjian HM, Sood AK, Lopez-Berestein G, Keating MJ, Fabbri M, and Calin GA (2017) Combining Anti-Mir-155 with Chemotherapy for the Treatment of Lung Cancers. Clin Cancer Res 23, 2891–2904 [PubMed: 27903673]
33. Elich M, and Sauer K (2018) Regulation of Hematopoietic Cell Development and Function Through Phosphoinositides. Front Immunol 9, 931 [PubMed: 29780388]
34. Tsantikos E, Lau M, Castelino CM, Maxwell MJ, Passey SL, Hansen MJ, McGregor NE, Sims NA, Steinfort DP, Irving LB, Anderson GP, and Hibbs ML (2018) Granulocyte-CSF links destructive inflammation and comorbidities in obstructive lung disease. J Clin Invest 128, 2406–2418 [PubMed: 29708507]
35. Maxwell MJ, Duan M, Armes JE, Anderson GP, Tarlinton DM, and Hibbs ML (2011) Genetic segregation of inflammatory lung disease and autoimmune disease severity in SHIP-1−/− mice. J Immunol 186, 7164–7175 [PubMed: 21572033]
36. Kurowska-Stolarska M, Alivernini S, Ballantine LE, Asquith DL, Millar NL, Gilchrist DS, Reilly J, Ierna M, Fraser AR, Stolarski B, McSharry C, Hueber AJ, Baxter D, Hunter J, Gay S, Liew FY, and McInnes IB (2011) MicroRNA-155 as a proinflammatory regulator in clinical and experimental arthritis. Proc Natl Acad Sci U S A 108, 11193–11198 [PubMed: 21690378]
37. Maxwell MJ, Srivastava N, Park MY, Tsantikos E, Engelman RW, Kerr WG, and Hibbs ML (2014) SHIP-1 deficiency in the myeloid compartment is insufficient to induce myeloid expansion or chronic inflammation. Genes Immun 15, 233–240 [PubMed: 24598798]
38. Musilova K, and Mraz M (2015) MicroRNAs in B-cell lymphomas: how a complex biology gets more complex. Leukemia 29, 1004–1017 [PubMed: 25541152]

39. Pena-Philippides JC, Caballero-Garrido E, Lordkipanidze T, and Roitbak T (2016) In vivo inhibition of miR-155 significantly alters post-stroke inflammatory response. J Neuroinflammation 13, 287 [PubMed: 27829437]

40. Yu X, Zheng Y, Zhu X, Gao X, Wang C, Sheng Y, Cheng W, Qin L, Ren N, Jia H, and Dong Q (2018) Osteopontin promotes hepatocellular carcinoma progression via the PI3K/AKT/Twist signaling pathway. Oncol Lett 16, 5299–5308 [PubMed: 30250599]

41. Evrard SM, Lecce L, Michelis KC, Nomura-Kitabayashi A, Pandey G, Purushothaman KR, d'Escamard V, Li JR, Hadri L, Fujitani K, Moreno PR, Benard L, Rimmele P, Cohain A, Mecham B, Randolph GJ, Nabel EG, Hajjar R, Fuster V, Boehm M, and Kovacic JC (2016) Endothelial to mesenchymal transition is common in atherosclerotic lesions and is associated with plaque instability. Nat Commun 7, 11853 [PubMed: 27340017]

42. Meadows KN, Iyer S, Stevens MV, Wang D, Shechter S, Perruzzi C, Camenisch TD, and Benjamin LE (2009) Akt promotes endocardial-mesenchyme transition. J Angiogenes Res 1, 2 [PubMed: 19946410]

43. Ambrozova G, Fidlerova T, Verescakova H, Koudelka A, Rudolph TK, Woodcock SR, Freeman BA, Kubala L, and Pekarova M (2016) Nitro-oleic acid inhibits vascular endothelial inflammatory responses and the endothelial-mesenchymal transition. Biochim Biophys Acta 1860, 2428–2437 [PubMed: 27431604]

44. Li J, Qu X, Yao J, Caruana G, Ricardo SD, Yamamoto Y, Yamamoto H, and Bertram JF (2010) Blockade of endothelial-mesenchymal transition by a Smad3 inhibitor delays the early development of streptozotocin-induced diabetic nephropathy. Diabetes 59, 2612–2624 [PubMed: 20682692]

45. Rawlings JS, Rosler KM, and Harrison DA (2004) The JAK/STAT signaling pathway. J Cell Sci 117, 1281–1283 [PubMed: 15020666]

46. Waters DW, Blokland KEC, Pathinayake PS, Burgess JK, Mutsaers SE, Prele CM, Schuliga M, Grainge CL, and Knight DA (2018) Fibroblast senescence in the pathology of idiopathic pulmonary fibrosis. Am J Physiol Lung Cell Mol Physiol 315, L162–L172 [PubMed: 29696986]

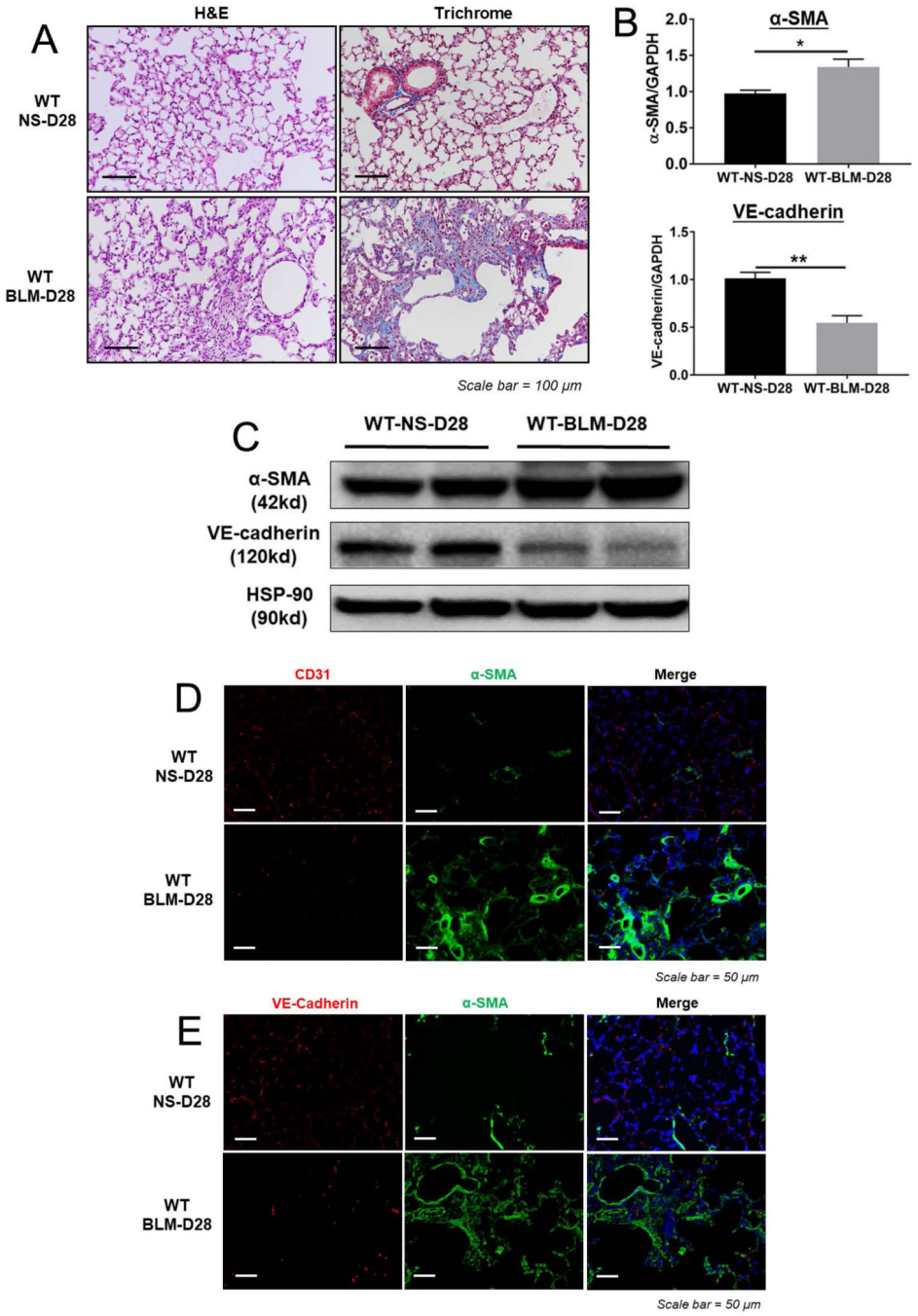

Figure 1. Endothelial-mesenchymal transition (EndoMT) was involved in BLM-induced lung fibrosis.

(A) Hematoxylin and eosin (H&E) and Masson's Trichrome stained lung sections from WT mice with BLM challenge or NS control for 28 days (WT-NS, WT-BLM, n=7–8 mice/group). (B) Q-PCR analysis of α-SMA and VE-cadherin mRNA in the lung tissues of WT-NS and WT-BLM mice. Results are Means±SEM from triplicate samples of 3 repeats. (C) Western blot of α-SMA and VE-cadherin proteins in the lung tissues of WT-NS and WT-BLM mice. HSP-90 was used for sample loading control. Shown are representative blots of 3 independent experiments. (D) Immunofluorescence of CD31 and α-SMA in WT-NS and

WT-BLM lung tissues and (E) Immunofluorescence of VE-Cadherin and α-SMA in WT-NS and WT-BLM lung tissues. Images were from different animals (n=7–8 mice/group). DAPI stained for nuclei (blue). *$p<0.05$, **$p<0.01$.

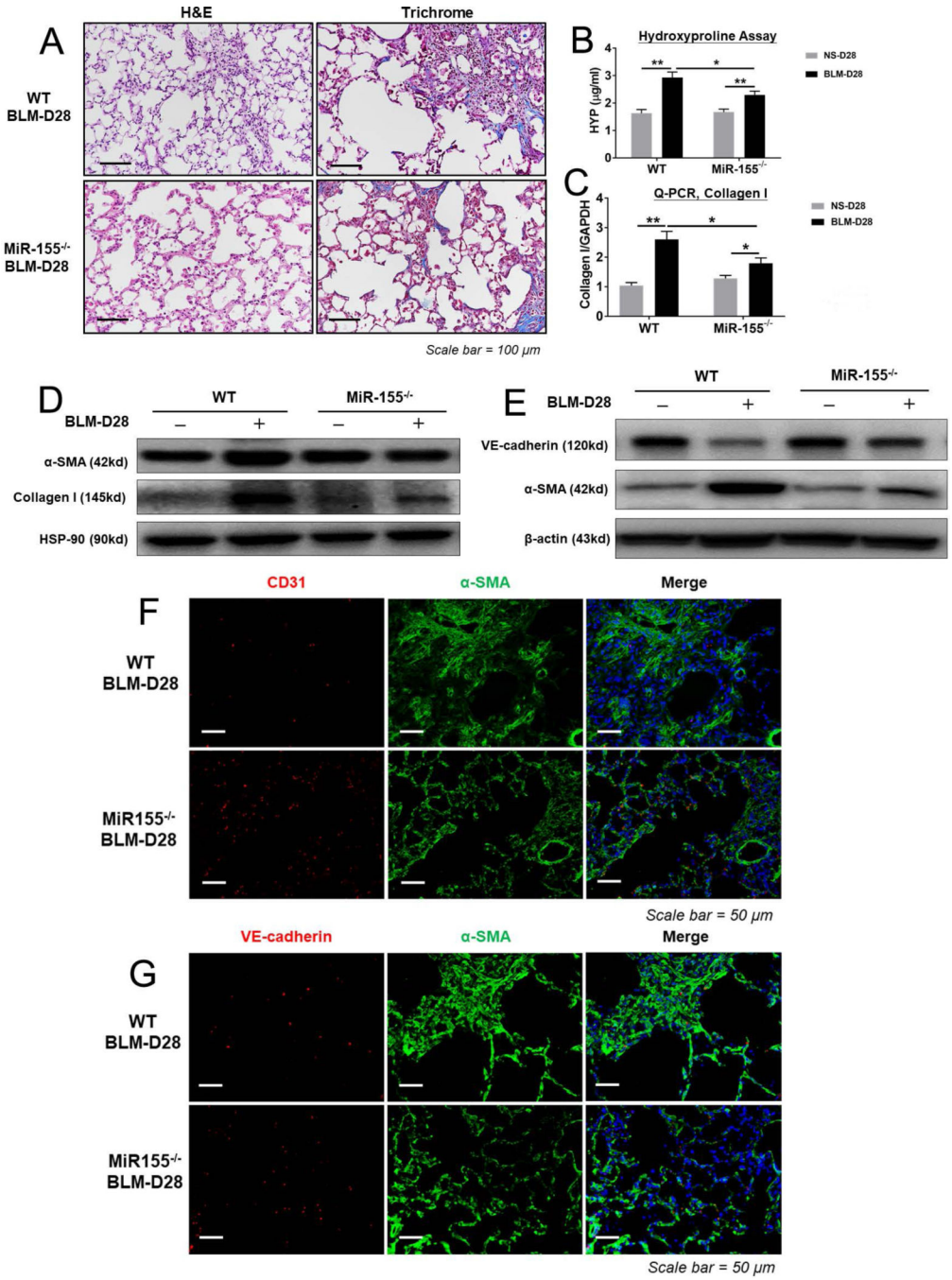

Figure 2. Deletion of MiR-155 alleviated fibrotic and EndoMT responses.

(A) H&E and Trichrome stained lung sections from WT and miR-155$^{-/-}$ mice with BLM stimulation for 28 days (WT-BLM, MiR-155$^{-/-}$-BLM, n=6–8 mice/group). (B) Hydroxyproline content in the lung tissues of WT and miR-155$^{-/-}$ mice challenged with NS or BLM (n=6–8 mice/group). (C) Q-PCR of Collagen I mRNA in WT and MiR-155$^{-/-}$ lung tissues after NS or BLM challenge. Results are presented as Means±SEM of triplicates of 3 repeats. (D, E) Western blots of α-SMA, Collagen I and VE-cadherin in the lung tissues of WT and miR-155$^{-/-}$ mice with or without BLM. HSP-90 or β-Actin as loading controls.

Shown are representative blots of 3 independent experiments. (F) Immunofluorescence of CD31 and α-SMA in WT-BLM and miR-155$^{-/-}$-BLM lung tissues. Images were from different aniamls (n=6–8 mice/group). (G) Immunofluorescence of VE-Cadherin and α-SMA in WT-BLM and miR-155$^{-/-}$-BLM lung tissues (n=6–8 mice/group). DAPI for nuclei (blue). *p<0.05; **p<0.01.

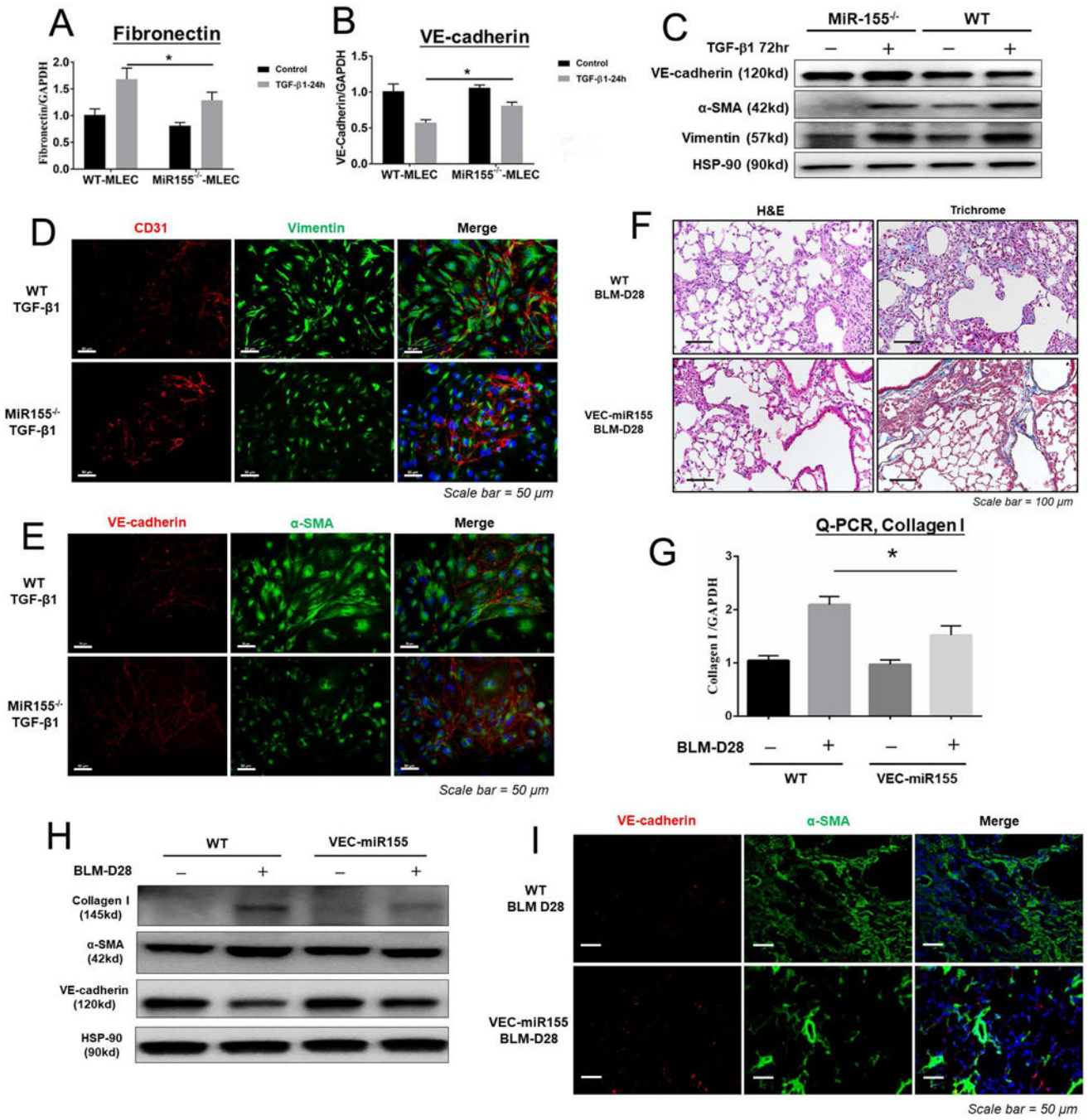

Figure 3. Role of endothelial MiR-155 in lung fibrosis.

(A, B) Q-PCR of Fibronectin and VE-cadherin mRNA in isolated MLEC from WT and MiR-155KO mice. Results are Mean±SEM of triplicates with 3 repeats. (C) Western blot of α-SMA, Vimentin and VE-cadherin in isolated WT and MiR-155KO MLEC stimulated with TGF-β1 for 72 hrs. Shown are representative blots from 3 independent experiments. (D, E) Immunofluorescence of CD31, Vimentin, VE-Cadherin, and α-SMA in MLEC after stimulation with TGF-β1. Results reprensent 3 independent experiments. (F) H&E and Trichrome staining of lung sections of WT and VEC-miR155 mice after BLM for 28 days

(n=6–8 mice/group). (G) Q-PCR of Collagen I mRNA in WT and VEC-miR155 mouse lungs with or without BLM. Results are Mean±SEM of triplicates with 3 repeats. (H) Western blot of Collagen I, α-SMA and VE-cadherin in WT and VEC-miR155 mouse lungs. Shown are representative blots of 3 independent experiments. (I) Immunofluorescence of VE-Cadherin and α-SMA in WT and VEC-miR155 mouse lungs (n=6–8 mice/group). DAPI for nuclei (blue). *$p<0.05$; **$p<0.01$.

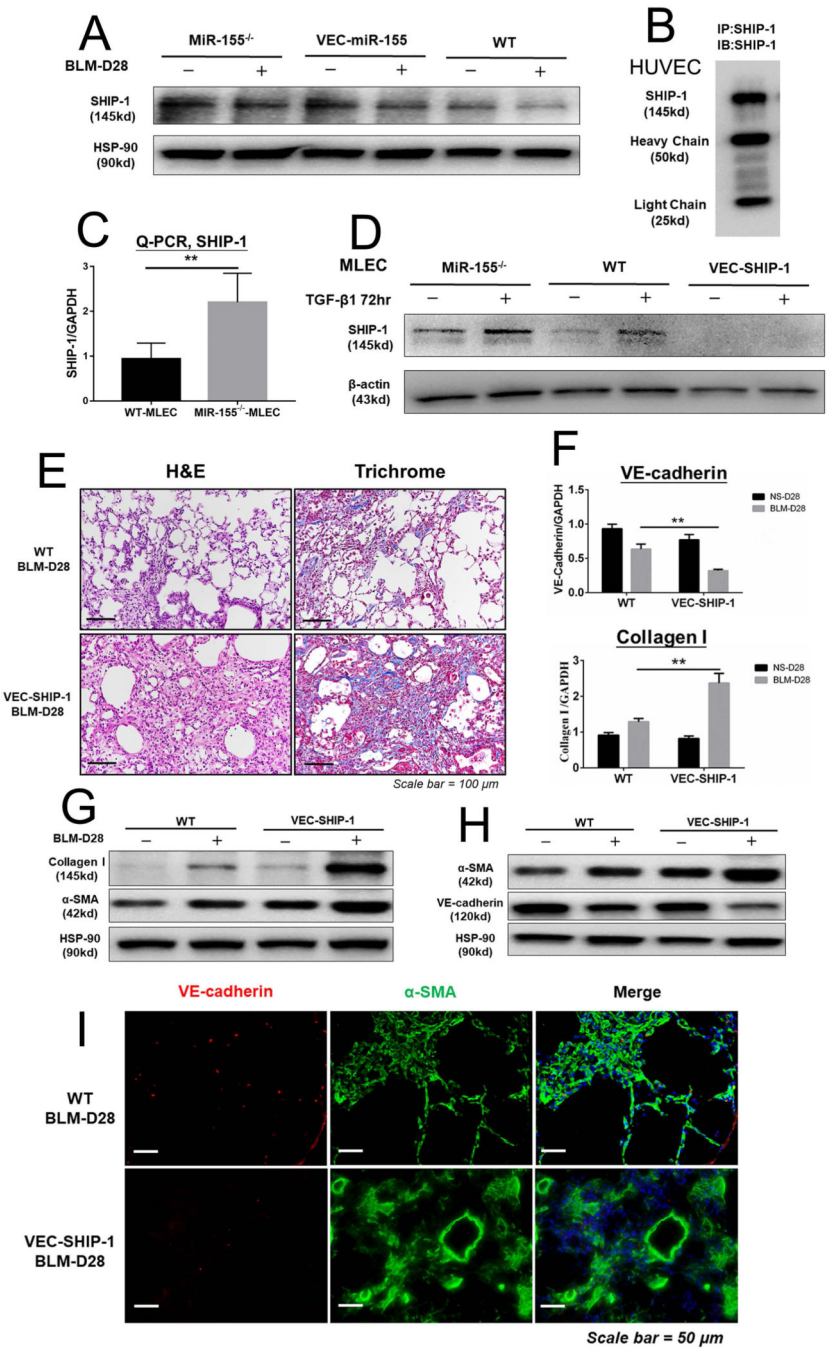

Figure 4. Lack of endothelial SHIP-1 facilitated lung fibrosis and EndoMT in vivo.

(A) Western blot of SHIP-1 in miR-155$^{-/-}$, VEC-miR-155 and WT mouse lungs before and after BLM challenge for 28 days (n=6 mice/group). (B) Immunoprecipitation (IP) and Western blot (IB) of SHIP-1 protein in HUVEC. Shown are representative results of 3 independent experiments. (C) Q-PCR of SHIP-1 mRNA in mouse lung endothelial cells (MLECs) from WT and VEC-miR155 mice before TGF-β1 stimulation. Results are Mean ±SEM of triplicates with 3 repeats. (D) Western blot of SHIP-1 in MLECs from miR-155$^{-/-}$, WT and VEC-SHIP-1 mice before and after TGF-β1 stimulation for 72 hrs. Results

represent 3 independent experiments. (E) H&E and Trichrome stained lung sections from WT and VEC-Cre-SHIP-1 (VEC-SHIP-1) mice after BLM challenge for 28 days (n=7–8 mice/group). (F) Q-PCR of Collagen I and VE-cadherin mRNA in WT and VEC- SHIP-1 mouse lungs. Results are Mean±SEM of triplicates with 3 repeats. (G) Western blot of Collagen I and α-SMA in WT and VEC-SHIP-1 mouse lung tissues and (H) Western blot of α-SMA and VE-cadherin in WT and VEC-SHIP-1 mouse lung tissues. Blots are representative results of 3 independent experiments. (I) Immunofluorescence of VE-Cadherin and α-SMA in WT and VEC-SHIP-1 mouse lung sections. Images were from different animals (n=6–8 mice/group). DAPI for nuclei (blue). *$p<0.05$; **$p<0.01$.

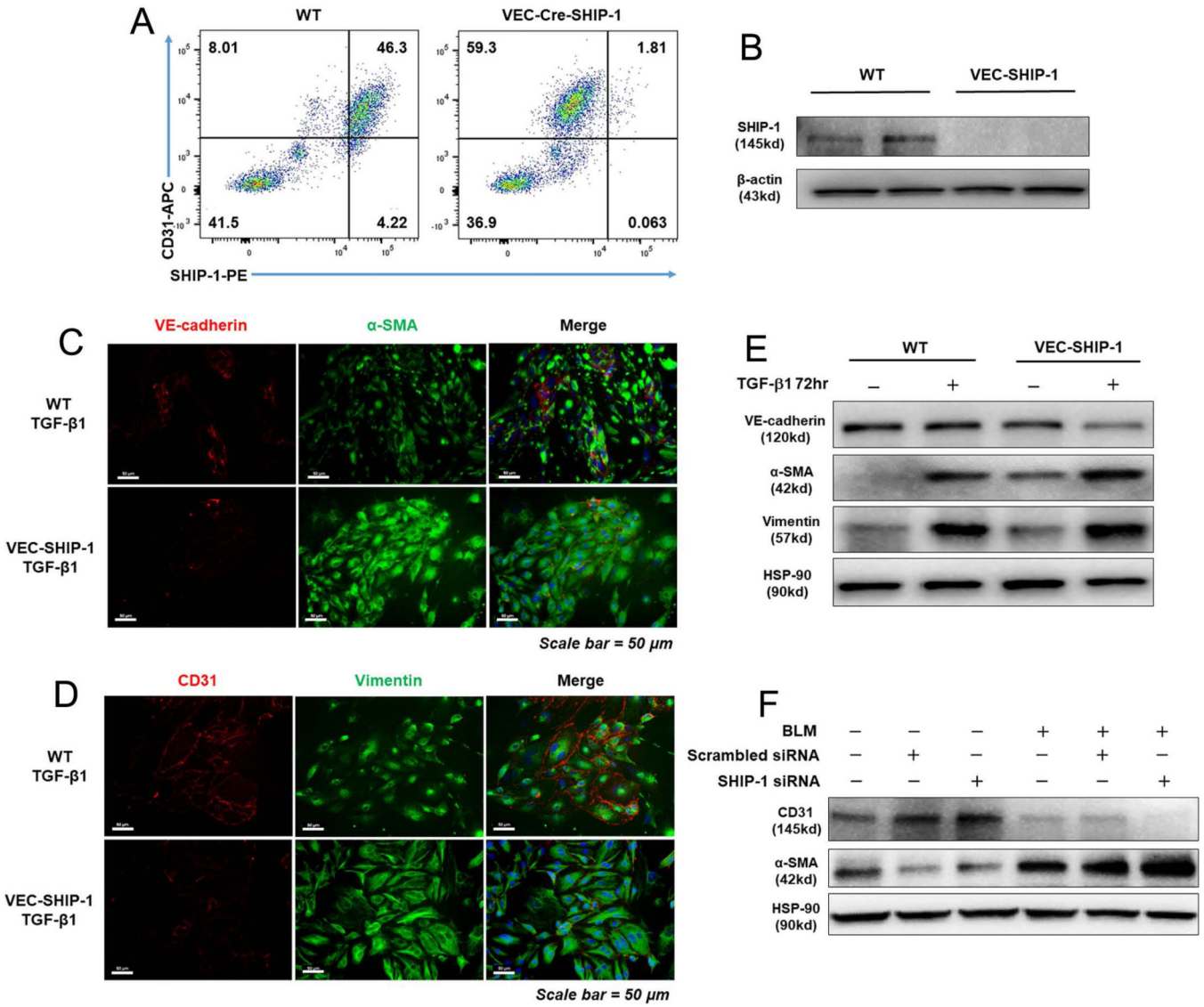

Figure 5. Effect of endothelial SHIP-1 on TGF-β1-induced EndoMT in vitro.

(A) Flow cytometry analysis of CD31 and SHIP-1 expression in isolated lung cells from WT and VEC-SHIP-1 mice. Upper right panels show the percentage of CD31 and SHIP-1 double positive cells. Results represent 3 independent experiments. (B) Western blot of SHIP-1 expression in WT and VEC-SHIP-1 mouse lung endothelial cells (MLECs). Shown is a representative blot of 3 separate experiments. (C) Immunofluorescence of VE-Cadherin and α-SMA in WT and VEC-SHIP-1 MLECs and (D) Immunofluorescence of CD31 and Vimentin in WT and VEC-SHIP-1 MLECs. Images were taken from 3 independent experiments. (E) Western blot of VE-Cadherin, α-SMA and Vimentin in WT and VEC-SHIP-1 MLECs with or without TGF-β1 stimulation for 72 hrs. Shown are representative results of 3 independent experiments. (F) Western blot of CD31 and α-SMA in primary HUVECs treated with siRNA to SHIP-1 or scrambled siRNA and with/without BLM for 72 hrs. Shown are representative results of 3 independent experiments.

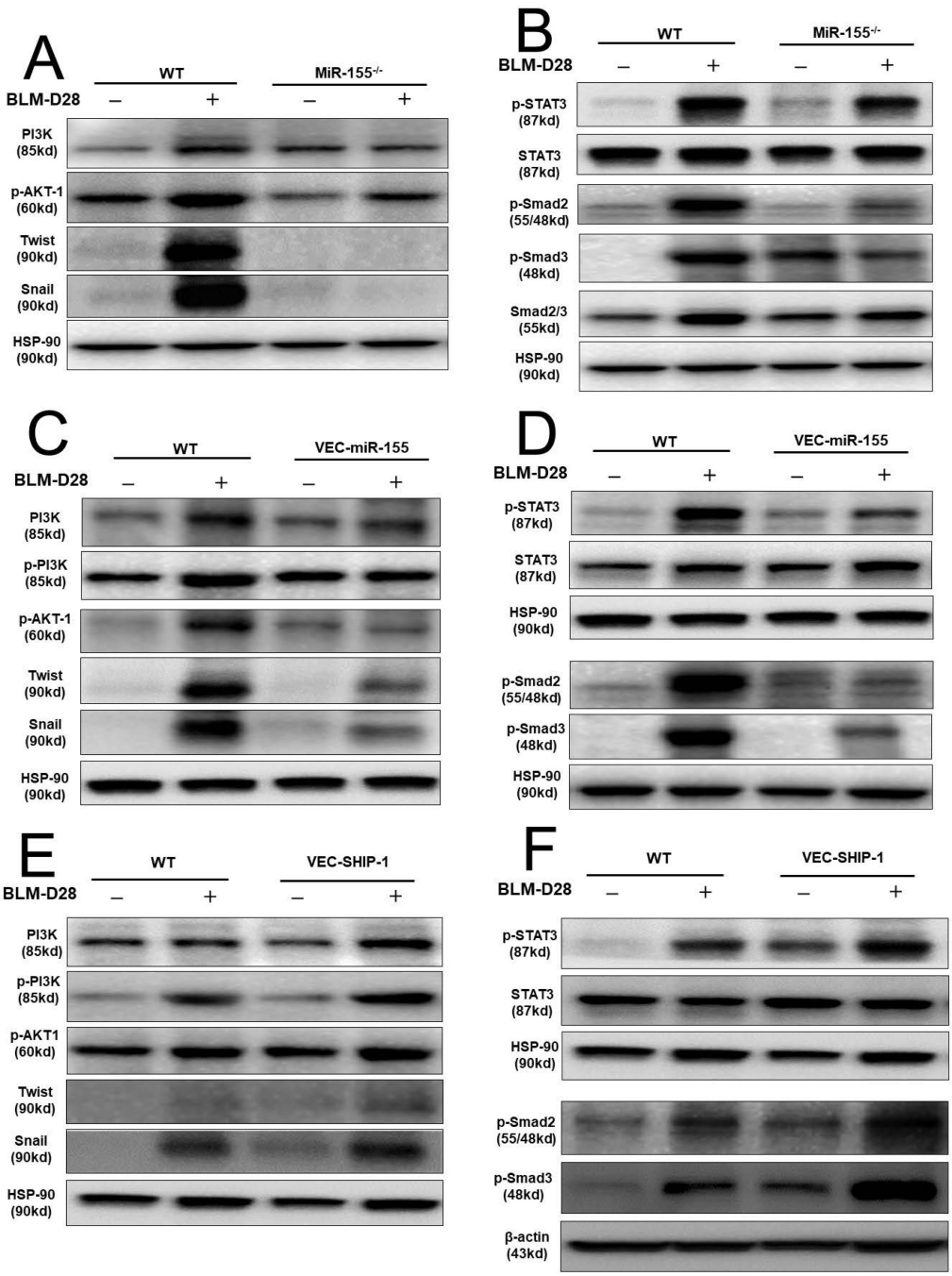

Figure 6. Endothelial miR-155 and SHIP-1 in pulmonary fibrosis involving PI3K/AKT, STAT3 and SMAD2/3 signaling pathways.

(A) Western blot of PI3K, p-AKT-1, Twist and Snail in WT and miR-155KO mouse lung tissues after BLM challenge for 28 days (n=6–8/group). (B) Expression of STAT3, Smad2/3 as well as activation of p-STAT3, p-Smad2, and p-Smad3 were detected by Western blot in WT and miR-155KO mice lung tissues (n=6–8/group). (C) Western blot of PI3K, p-PI3K, p-AKT-1, Twist and Snail in WT and VEC-miR-155 mice lung tissues (n=6–8/group). (D) Expression of STAT3 as well as activation of p-STAT3, p-Smad2, and p-Smad3 in WT and VEC-miR-155 mouse lung tissues were analyzed by Western blot (n=6–8/group). (E)

Protein expression of PI3K, Twist, Snail as well as activation of p-PI3K, and p-AKT1 in WT and VEC-SHIP-1 mouse lung tissues (n=6–8/group). (F) Western blot of p-STAT3, STAT3, p-SMAD2 and p-SMAD3 in WT and VEC-SHIP-1 mouse lung tissues (n=6–8/group).

Table 1.

Primer Sequences Used for qPCR Analyses

Gene	Sequences (5’−3’)
α-SMA-F	CCAGCACCATGAAGATCAAG
α-SMA-R	TTCGTCGTATTCCTGTTTGC
VE-Cadherin-F	TCCTCTGCATCCTCACTATCACA
VE-Cadherin-R	GTAAGTGACCAACTGCTCGTGAAT
Collagen I-F	CATAAAGGGTCATCGTGGCT
Collagen I-R	TTGAGTCCGTCTTTGCCAG
Fibronectin-F	GACTCATGGTGGCACTAAATA
Fibronectin-R	CTTCTTGGAGGGCTAACATTCT
SHIP-1-F	CAGGGATGAAGTACAACTTGCC
SHIP-1-R	TCTCCTTCCTGACTCTTGACA
GAPDH-F	ACAACTTTGGCATTGTGGAA
GAPDH-R	GATGCAGGGATGATGTTCTG